
# Harmonic Instability Analysis of Single-Phase Grid Connected Converter using Harmonic State Space (HSS) modeling method

Kwon, Jun Bum; Wang, Xiongfei; Bak, Claus Leth; Blaabjerg, Frede

*Published in:*
Proceedings of the 2015 IEEE Energy Conversion Congress and Exposition (ECCE)

*DOI (link to publication from Publisher):*
10.1109/ECCE.2015.7310001

*Publication date:*
2015

*Document Version*
Accepted author manuscript, peer reviewed version

# Harmonic Instability Analysis of Single-Phase Grid Connected Converter using Harmonic State Space (HSS) modeling method

JunBum Kwon, Xiongfei Wang, Claus Leth Bak, Frede Blaabjerg
Department of Energy Technology
Aalborg University
Aalborg, Denmark
E-mail : jbk, xwa, clb, fbl @et.aau.dk

***Abstract –The increasing number of renewable energy sources at the distribution grid is becoming a major issue for utility companies, since the grid connected converters are operating at different operating points due to the probabilistic characteristics of renewable energy. Besides, typically, the harmonics and impedance from other renewable energy sources are not taken carefully into account in the installation and design. However, this may bring an unknown harmonic instability into the multiple power sourced system and also make the analysis difficult due to the complexity of the grid network. This paper proposes a new model of a single phase grid connected renewable energy source using the Harmonic State Space modeling approach, which is able to identify such problems and the model can be extended to be applied in the multiple connected converter analysis. The modeling results show the different harmonic impedance matrixes, where that represents the harmonic coupling characteristic as well as the different instability characteristics. The theoretical modeling and analysis are verified by simulations and also experimental results.***

*Keywords—Harmonic State Space Modeling, Single-phase grid connected converter, Harmonic instability, Harmonic analysis, Harmonic coupling.*

## I. INTRODUCTION

The installation rate of renewable energy sources is drastically increasing both for home applications but also in large plants [1-3]. Especially, photovoltaic systems, which are installed on the roof of houses as well as in windows of building, are rapidly growing [1, 4-7]. In the beginning of these renewable energy installations, the single-phase grid connected converter having a small power capacity was not an issue for the grid. However, it has now become a more critical issue in terms of power quality and stability problems [2, 8-10] because many units are now installed.

To mitigate harmonics from inside and outside of the converter, many studies have been done [11, 12]. Most of them are focusing on the mitigation methods by means of PI controller based systems using the rotating frame or Proportional Resonant (PR) controllers [11, 12]. Besides, there are a few studies, which are talking about the analysis of harmonic in multiple connected renewable energy sources [3]. Even if they tried to analyze the final output harmonics, most of approaches were based on direct measuring or using probabilistic or stochastic results [3]. The main reasons for the difficulties of the analysis are that every harmonic component has its own varying phasor characteristic, which can influence the other converters [13]. Furthermore, the impedance characteristics of the converter have also varying phasor characteristics. Therefore, the harmonic can be canceled, attenuated or sometimes, amplified according to the load flow and operation of each converter in the same grid. Hence, it is required to develop an accurate tool and model, which can be used not only for the analysis of harmonic origin, but also be combined with other converter models easily.

On the contrary to the traditional modeling approach [14, 15], the Harmonic State Space (HSS) modeling method is introduced in power system studies to analyze the harmonic coupling and stability in a large power network [16, 17]. The main characteristics of this model can be explained in two ways. First, this modeling approach is based on the Linear Time Periodic (LTP) theory, where this concept has been widely applied in mechanical and civil engineering to include the time varying signal and to analyze the vibrations in the system [18, 19]. Hence, it can also include time-varying harmonic terms in the electrical model by the same method. Second, the switching component, which is normally aggravated into a constant value in the Linear Time Invariant (LTI) model, can be included as a harmonic phasor vector by means of FFT [16]. The derived results can show the coupling of dynamic transfer function as well as the coupling of the steady-state impedance phasor in the matrix.

This paper presents the modeling and analysis of a single phase grid connected converter for renewable energy source by means of HSS modeling. The detailed modeling procedure is described with the background of the HSS theory. Besides, the obtained harmonic transfer function is analyzed for the dynamic harmonic phasor response using eigenvalue analysis. In order to represent the steady-state harmonic coupling inside and outside of the converter model, the harmonic impedance phasor matrix is analyzed, where this is also derived from the HSS model. Consequently, all the analyzed results are verified by the time-domain simulation and the developed HSS model. Besides, experiments are performed to verify the obtained harmonic transfer function.

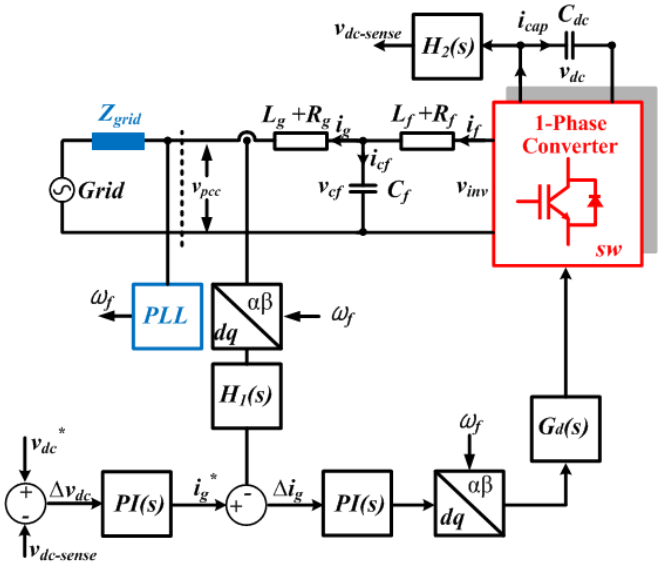


Fig 1. Block diagram of single-phase grid connected PWM converter.

## II. HSS Modeling Of Single Phase Grid Connected Converter

A generalized single phase grid connected converter is considered in the modeling procedures and the basic structure of the converter is shown in Fig. 1, where $L_f$, $C_f$, $L_g$, $C_{dc}$, $Z_{grid}$ are the converter side inductor, capacitor filter, grid side inductor, dc-link capacitor and grid impedance, respectively. The dc-link voltage is controlled by a PI controller using the feedback filtered ($H_2(s)$) signal. The derived current reference ($i_g^*$) is also controlled by a PI controller, where the transformed grid current is filtered by a low pass filter ($H_1(s)$). The final reference signal, which is divided by the dc voltage, is compared with the carrier signal in order to generate the PWM (sw) signals. The detailed procedure for transforming the LTI model to LTP model is as follows:

### *A. Review of HSS modeling*

The HSS modeling is based on the assumption that all signals are varying periodically in time. If the state transition matrix, input signals and output signals are varying, they can not be solved by the general state space equation. As, the LTI state space equation is solved in the linearized operating point, which means that the state-transition matrix as well as parameter matrix of system are also fixed. Hence, it is needed to be linearized, where this model is linearized according to the time-varying trajectories. Based on this theory, all the time-domain signals ($x(t)$) can be represented into (1) in the interval $[t_0, t_0 + T]$, where T is the period of signal, $X_k$ is the Fourier coefficient, $\omega_0$ is the angular frequency and k is the harmonic order.

$$x(t) = \sum_{k\in\mathbb{Z}} X_k e^{jk\omega_0 t} \tag{1}$$

Additionally, in order to include dynamic performance in the time and frequency domain, it is required to use the

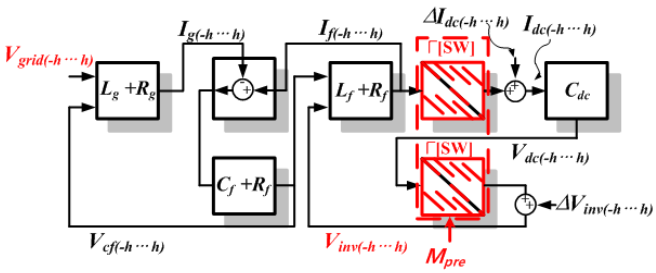


Fig 2. Block diagram of LTP topology model.

Exponentially Modulated Periodic (EMP) function as the kernel function ($e^{-st}$) as shown in (2).

$$x(t) = e^{st} \sum_{k\in Z} X_k e^{jk\omega_0 t} \tag{2}$$

Based on the basic representation of the EMP signal characteristics, it is also possible to derive various mathematical expressions like the derivative, integral and the product of two signals in order to make a time varying differential equation of the power converter. Finally, the HSS equation is shown in (3), which has a time varying state transition matrix ($A - N$) and a time varying state variable matrix (X), which can be represented into the production of the matrix.

$$\begin{aligned} (s + jm\omega_0)X_n &= \sum_{-\infty}^{\infty} A_{n-m}X_m + \sum_{-\infty}^{\infty} B_{n-m}U_m \\ Y_n &= \sum_{-\infty}^{\infty} C_{n-m}X_m + \sum_{-\infty}^{\infty} D_{n-m}U_m \end{aligned} \tag{3}$$

The important thing is that all matrix row and column are in the frequency domain, where they can be converted into the time domain by means of (4)

$$x(t) = \Gamma(t)X \tag{4}$$

where,

$$\Gamma(t) = [e^{-jh\omega_0 t} \cdots e^{-j2\omega_0 t}, e^{-j\omega_0 t}, 1, e^{j\omega_0 t}, e^{j2\omega_0 t} \cdots e^{jh\omega_0 t}]$$
$$X = [X_{-h}(t) \cdots X_{-1}(t) X_0(t) X_1(t) \cdots X_h(t)]^T$$

### *B. Topology modeling*

According to the introduced model (1) ~ (4) and the basic circuit theory, the HSS model for a single-phase grid connected converter using an *LCL* filter can be obtained as shown in (5) and Fig. 2.

$$\begin{bmatrix} \dot{I_g}(t) \\ \dot{I_f}(t) \\ \dot{V_{cf}}(t) \\ \dot{V_{dc}}(t) \end{bmatrix} = \begin{bmatrix} \frac{-R_g}{L_g}I - N & Z_M & \frac{-1}{L_g}I & Z_M \\ Z_M & \frac{-R_f}{L_f}I - N & \frac{1}{L_f}I & -\frac{\Gamma[SW^T]}{L_f} \\ \frac{1}{C_f}I & \frac{-1}{C_f}I & -N & Z_M \\ Z_M & \frac{\Gamma[SW]}{C_{dc}} & Z_M & -N \end{bmatrix} \begin{bmatrix} I_g(t) \\ I_f(t) \\ V_{cf}(t) \\ V_{dc}(t) \end{bmatrix} + \begin{bmatrix} \frac{1}{L_g}I & Z_M & Z_M & Z_M \end{bmatrix} \begin{bmatrix} V_{pcc}(t) \\ Z_M \\ Z_M \\ Z_M \end{bmatrix} \tag{5}$$

where, the acronyms can be found in Fig. 1. "*I*" means the identity matrix, "*N*" means the dynamic matrix, which is derived from (3) and "$Z_M$" is the zero matrix. The small letter in Fig. 1 means the time domain signal. On the other hand, the

capital letters in (5) stands for the harmonic coefficient component as shown in Fig. 1, which is derived from the Fourier series (1). The results from (5) can be re-transformed into the time by means of (4). Additionally, the size of each matrix depends on the number of harmonics considered in the model. It is noted that the -20$^{th}$ ~20th harmonics, the switching harmonics and the sideband harmonics are considered in the model as given in (6).

$$\mathrm{h} = [\dots, -h_{sw}, -h_{sw+1}, -20, \dots, -1,0,1, \dots, 20, \dots h_{sw-1}, h_{sw}, \dots] \quad (6)$$

According to the PWM strategy, e.g., bipolar or unipolar Sinusoidal PWM (SPWM), the frequency and the magnitude of the side band and harmonics can be determined. The time domain switching function can be reorganized into a Toeplitz ( $\Gamma$ ) [18] matrix as given by (7) in order to perform a convolution, where the product of two time domain signals are exactly the same as the convolution of two frequency domain signals. The Fourier coefficient of the steady-state switching ($\dots \mathrm{SW}_{-2}, SW_{-1}, SW_0, SW_1, SW_2 \dots$) can be obtained from the direct FFT of the time domain simulation or the analytical model, e.g., Bessel function. The dynamic variation of the switching can be updated by adding the small variation of switching, which is achieved from the controller, to the previous switching matrix (SW(t)).

$$\mathrm{SW(t)} = \begin{bmatrix} SW_0 & SW_{-1} & SW_{-2} & \dots \\ SW_1 & SW_0 & SW_{-1} & \dots \\ SW_2 & SW_1 & SW_0 & \dots \\ \vdots & \vdots & \vdots & \ddots \end{bmatrix} \quad (7)$$

*C. Controller modeling*

To take into account the decomposed harmonics in the controller, a low-pass filter and PI-controller can also be transformed by means of the frequency shift as given in (8) and (9).

$$\mathrm{PI} = \begin{bmatrix} PI(s - jh\omega_0) & & & \\ & \ddots & & \\ & & PI(s) & \\ & & & \ddots \\ & & & PI(s + jh\omega_0) \end{bmatrix} \quad (8)$$

where, $\mathrm{PI(s)} = \mathrm{K_p} + K_i/s$, $\mathrm{K_p}$ is the proportional gain and $\mathrm{K_I}$ is the integrator gain.

$$\mathrm{H_1, H_2} = \begin{bmatrix} H(s - jh\omega_0) & & & \\ & \ddots & & \\ & & H(s) & \\ & & & \ddots \\ & & & H(s + jh\omega_0) \end{bmatrix} \quad (9)$$

where, $\mathrm{H(s)} = 1/(\mathrm{s} \cdot \mathrm{K_{lpf}} + 1)$, $\mathrm{K_{lpf}}$ is the low pass filter bandwidth. This shifted transfer function show the dynamic behavior of each harmonics by using the multiplication and convolution.

In order to include the controller behavior into (5), it is required to put the small variation terms of the switching ($\Delta[\mathrm{SW}]$) into the base value ($\Gamma[SW]_{base}$), where the small variation terms are zero, if there is not variation of the

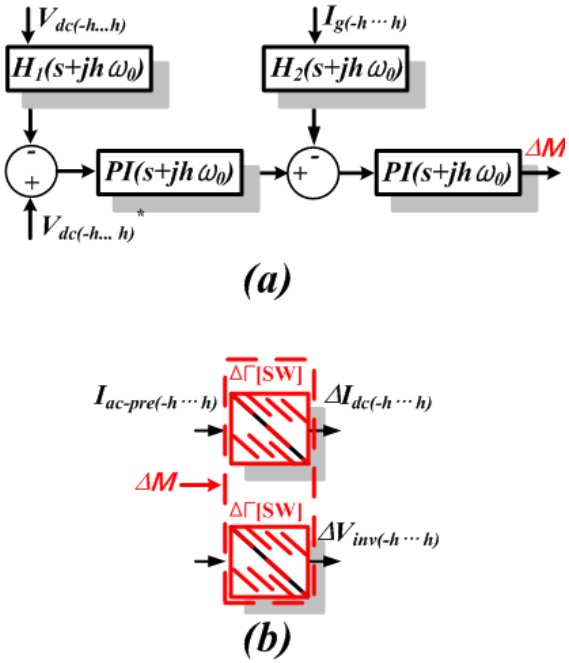


Fig 3. Block diagram of LTP controller model
(a) Low-pass filter and PI controller, (b) Switching matrix to update the nonlinear switching from the previous state.

controller. Hence, the small variation ($\Delta[\mathrm{SW}]$) given by the controller should be multiplied and added with the previous dc voltage ($\mathrm{V_{dc-pre}}$) and ac current ($I_{\mathrm{ac-pre}}$) through (10).

$$\begin{aligned} \Delta\mathrm{V_{inv}} &= \Gamma[SW]_{base}\Delta\mathrm{V_{dc}} + \Delta[\mathrm{SW}]\,\Gamma\left[\mathrm{V_{dc-pre}}\right] \\ \Delta\mathrm{I_{dc}} &= \Gamma[SW]_{base}\Delta\mathrm{I_{ac}} + \Delta[\mathrm{SW}]\,\Gamma\left[I_{\mathrm{ac-pre}}\right] \end{aligned} \quad (10)$$

where, "$\Delta$" term means the small variation of each signal, which is obtained from the partial differential equation of (5). Especially, a small variation of the switching component ( $\Delta[\mathrm{SW}]$ ) is achieved from the convolution between the controller output and the partial differential equation of the switching matrix. The acronym "-pre" means the previous state value calculated from (5). Conclusively, the small variation of nonlinear-discontinuous signal (sw(t)) can be linearized as given in (10).

In the case of a time domain model, the single-phase signal is normally delayed by means of the all pass filter in order to obtain the αβ signal. However, in the case of HSS model, the measured grid current ($\mathrm{i_g}$) is transformed into αβ frame by multiplying the complex number (j) to the Fourier coefficient ($\mathrm{I_g}$) of the grid current as given by (11) because all signals of the HSS model are composed by the Fourier coefficient, which means they are composed by the complex number.

$$\mathrm{I_\beta} = [I_{\alpha(-h)} \cdot j, I_{\alpha(h)} \cdot -j] \quad (11)$$

The αβ-dq transformation can also be performed by using the complex number. The Park transformation, which is decomposed by means of the Fourier series, is as given in (12).

$$Park_{HSS} = \begin{bmatrix} \Gamma\left[\frac{1}{2} \quad 0 \quad \frac{1}{2}\right] & \Gamma\left[-\frac{1}{2i} \quad 0 \quad \frac{1}{2i}\right] \\ -\Gamma\left[-\frac{1}{2i} \quad 0 \quad \frac{1}{2i}\right] & \Gamma\left[\frac{1}{2} \quad 0 \quad \frac{1}{2}\right] \end{bmatrix} \quad (12)$$

ex) $\mathrm{Park_{HSS}} \cdot \begin{bmatrix} 0.5n \\ 0 \\ 0.5n \\ 0.5ni \\ 0 \\ -0.5ni \end{bmatrix} = \begin{bmatrix} 0 \\ n \\ 0 \\ 0 \\ 0 \\ 0 \end{bmatrix}$, where n=peak value of $\mathrm{i_g}$

According to the convolution rules used in the modeling theory, the structure has a Toeplitz formation. The final obtained result is a real number (A). If this value is converted to the time domain by using (4), the result is the same with the Park transformed signal in the time domain.

In another way, the dq information can be achieved by adding the fundamental Fourier coefficient of the grid current ($\mathrm{I_d} = I_{g1} + I_{g-1}, I_q = 0$) based on the assumption that the q-axis component is controlled to be "0". The PLL dynamics is neglected in this case in order to focus on the effect of the time-varying PWM. Hence, the sine and cosine information are assumed to be a synchronized value with the grid voltage. According to these characteristics, a full HSS model can be obtained.

## III. Analysis Of Harmonic Coupling And Instability

### *A. Harmonic Transfer Function*

Describing both the steady-state and dynamic harmonic coupling is possible by means of (3), where it can be converted into the harmonic transfer function ($\mathrm{H_k}(s)$) format for each harmonic component (k) as shown in (13).

$$\mathrm{H_k}(s) = \sum_l \hat{C}_{k-l} \left((s + jl\omega_0)I - \hat{A}\right)^{-1} \hat{B}_l + D_k \quad (13)$$

$$\mathrm{H(s)} = \begin{bmatrix} \ddots & \vdots & \vdots & \vdots & \\ \dots & H_0(s-j\omega) & H_{-1}(s) & H_{-2}(s+j\omega) & \dots \\ \dots & H_1(s-j\omega) & H_0(s) & H_{-1}(s+j\omega) & \dots \\ \dots & H_2(s-j\omega) & H_1(s) & H_0(s+j\omega) & \dots \\ & \vdots & \vdots & \vdots & \ddots \end{bmatrix} \quad (14)$$

where, $\hat{B}_k$, $\hat{C}_k$, and $\mathrm{D_k}$, are the Fourier coefficients of the periodic functions $\hat{B}(t)$, $\hat{C}(t)$, and $\mathrm{D(t)}$, respectively. At this point, $\mathrm{H(s)}$ is a double infinite matrix defined as (14), where it defines the coupling among different frequencies. When "s" is equal to "0", it will give the steady state harmonic coupling status. On the contrary, the results can express the dynamic interaction between the coupled harmonic transfer functions, if "s" is not "0". Hence, this characteristic is appropriate to demonstrate the stability and impedance coupling characteristic, which can not be identified in the conventional LTI model.

### *B. Steady-state harmonic interaction*

Based on the derived harmonic transfer function (14), the full model given in (5)-(12) is analyzed. In the steady state, the derivative term of (5)-(12) is zero. Hence, the control dynamics can be neglected, where the switching matrix ( $\Gamma[\mathrm{SW}]$ ) is including the information of the controlled modulation. As the final modulation signal from the controller will not change in steady state. Hence, the base matrix of the switching ($\Gamma[\mathrm{SW}]$), which is derived from the steady state modulation in the controller, is enough to analyze the steady state harmonics.

As a result, (14) can be represented as $\mathrm{Y(s)} = \sum_{k=-\infty}^{\infty} H_k(s - jk\omega_0)U(s - jk\omega_0)$, where $\mathrm{U(s)} = [\dots U(s - jk\omega_0)\ U(s)\ U(s + jk\omega_0) \dots]^T$ , $\mathrm{Y(s)}$ can also be represented analogously. Hence, the steady-state harmonic coupling between the input and output harmonics can be described as shown in (15), when "s" is equal to "0".

$$\begin{aligned} Y_{-1}(-j\omega) = & \dots \mathrm{H_0}(-j\omega)U_{-1}(-j\omega) + H_{-1}(0)U_0(0) \\ & + H_{-2}(+j\omega)U_1(+j\omega) \dots \\ Y_0(0) = & \dots \mathrm{H_1}(-j\omega)U_{-1}(-j\omega) + H_0(0)U_0(0) \\ & + H_{-1}(+j\omega)U_1(+j\omega) \dots \\ Y_1(+j\omega) = & \dots \mathrm{H_2}(-j\omega)U_{-1}(-j\omega) + H_1(0)U_0(0) + \\ & H_0(+j\omega)U_1(+j\omega) \dots \end{aligned} \quad (15)$$

All harmonic impedances ($\mathrm{H_k(0)}$) are composed of complex number, which means the matrix information are phasors synthetized from the HSS model in (5)-(12).

### *B. Dynamic harmonic interaction and stability*

The dynamics of the coupled HTF can easily be analyzed by using the traditional LTI analysis method [19]. In this paper, a Pole-Zero mapping is used as a tool to identify which poles and zeros make instability problems at each operating point and it is given by (16).

$$\mathrm{H_k}(s + jk\omega) = \frac{N_k(s+jk\omega)}{D_k(s+jk\omega)} \quad (16)$$

If the pole of one specific HTF is on the Right Half Plane (RHP), the time response of that harmonics will increase, exponentially and it can make the whole system in the unstable. Furthermore, a closed loop Bode diagram can be drawn by using (14), where the diagram can show which harmonic impedance are coupled with different magnitudes at each operating points.

## IV. Simulation And Experimental Result

MATLAB and PLECS tools are used to compare the modeling results with non-linear time domain simulation. The derived HSS model in (5)-(12) is solved by means of an m-file script. Besides, laboratory tests are also performed in an experimental set-up, where a single-phase frequency drive is used as a grid connected converter with an LCL-filter. The control algorithms for the experiments are implemented in a DS1007 dSPACE system.

In the case of steady state harmonics, the results can be obtained by using (15). On the other hand, the same results can also be obtained from (14). In the case of the single phase converter, the dc-side harmonics ( $\omega_r, 2\omega_r, 4\omega_r \dots$ ) can be transferred into the ac-side using shifted frequencies ($\omega_r \pm 1, 2\omega_r \pm 1, 4\omega_r \pm 1 \dots$), which is dependent on the modulation procedure of the converter topology. Even though the input

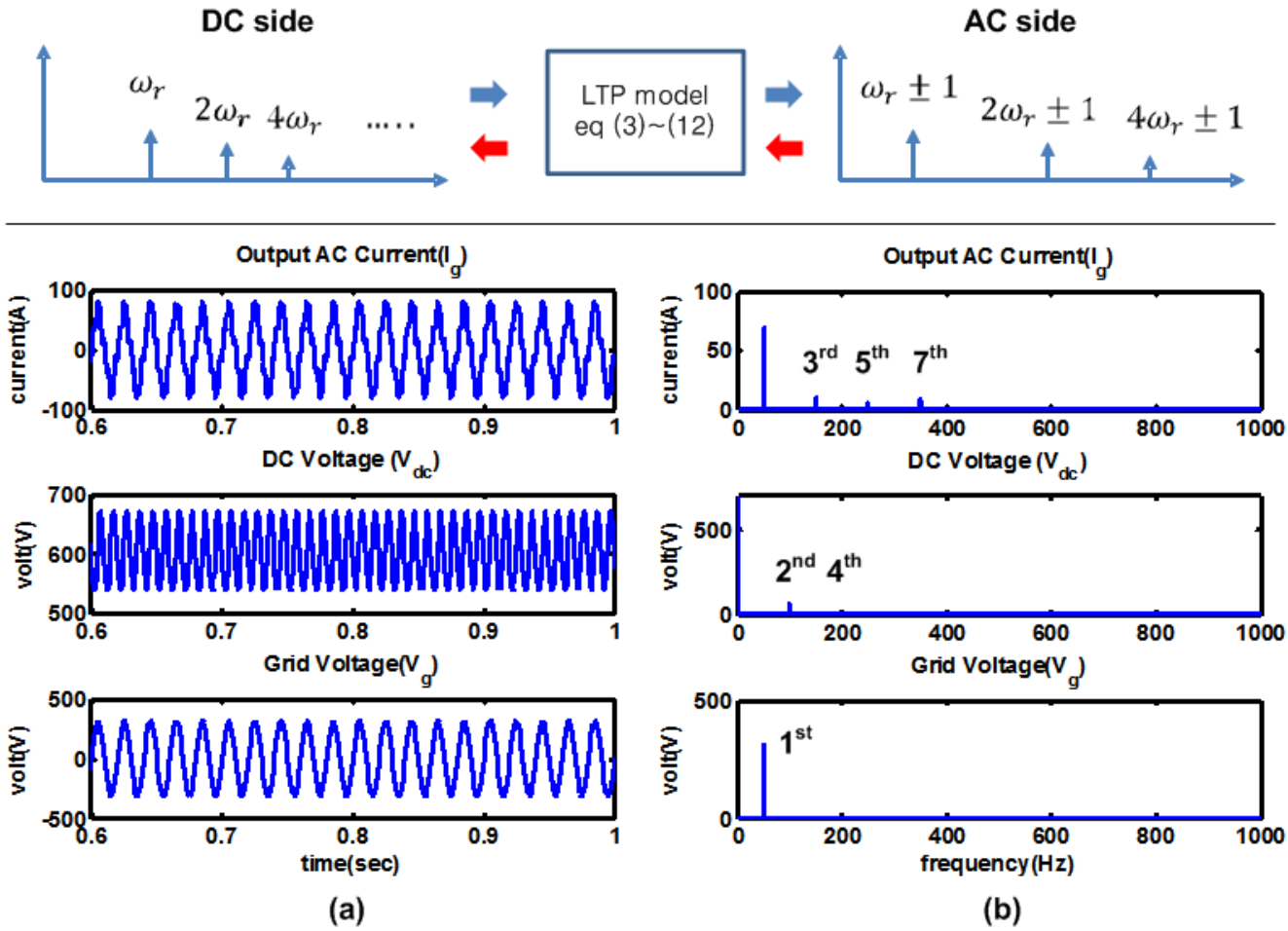


Fig 4. Simulation result of single phase grid connected converter at steady state (10 kW)
(a) Time domain simulation results of HSS model, (b) FFT simulation results of HSS model

grid voltage is not distorted, the grid current has a distorted current waveform due to both the modulation procedure and the dc-side harmonics as shown in Fig. 4, where $\omega_r$ is the fundamental frequency of the harmonics. The generated harmonics between the ac-side and the dc-side are well matched with the theory as shown in Fig. 4.

Simulations of the dynamic behavior are also performed by using the HSS model. For the simplicity of the analysis, -3rd ~ 3rd harmonics are considered in the HSS model. As shown in Fig. 5-(a), (c), the dc voltage ($V_{dc}$) is stable, when the voltage controller gain is "$K_p$=0.5". The result is matching well with the pole-zero mapping of the HSS model, where all poles of HSS model are in the left half plane. However, the system is being unstable, when the $K_p$ gain is increasing. Furthermore, the pole-zero mapping shows also the unstable state, where two poles in the 2nd order harmonic transfer function are in the right half plane as shown in Fig. 5-(b), (d). However, the poles of the other harmonics are still in the left half plane and thereby stable. The Fig. 6 shows the time domain results of the analyzed system. As in the analysis with the pole-zero mapping, the response of the second order harmonics at the dc side has an unstable response as shown in Fig. 6-(a). It is also seen that the other harmonics are stable, even they have oscillations. Furthermore, the unstable response of the 2nd order harmonic is directly transferred to the ac side due to the frequency shift, which is introduced in the steady-state harmonic analysis. As a result it can be found that the responses of the 1st and 3rd harmonic transfer function at the ac-side are unstable. However, the 2nd order harmonic is convergent as shown in Fig. 6-(b).

An experimental validation is verified by means of signal processing. The test set-up is composed of three stages as shown in Fig. 7. First, the hardware platform is done by a single phase frequency drive. Second, the converter is controlled by dSPACE system, where the dc voltage ($v_{dc}$), the grid voltage ($v_{pcc}$) and the grid current ($i_g$) are directly measured from the hardware set-up. In order to verify the HTF method, the number of the transfer functions depends on the number of harmonics considered in the whole model. The third stage in this paper is to simulate the same dynamic result same as shown in the experimental results.

From the control desk of the dSPACE system, the time-domain data are acquired by means of a record function. The inverter-side filter current, capacitor voltage, the state of the PI controller, PWM signals, and the grid voltage are the measured signal s. The recorded time-domain signals are

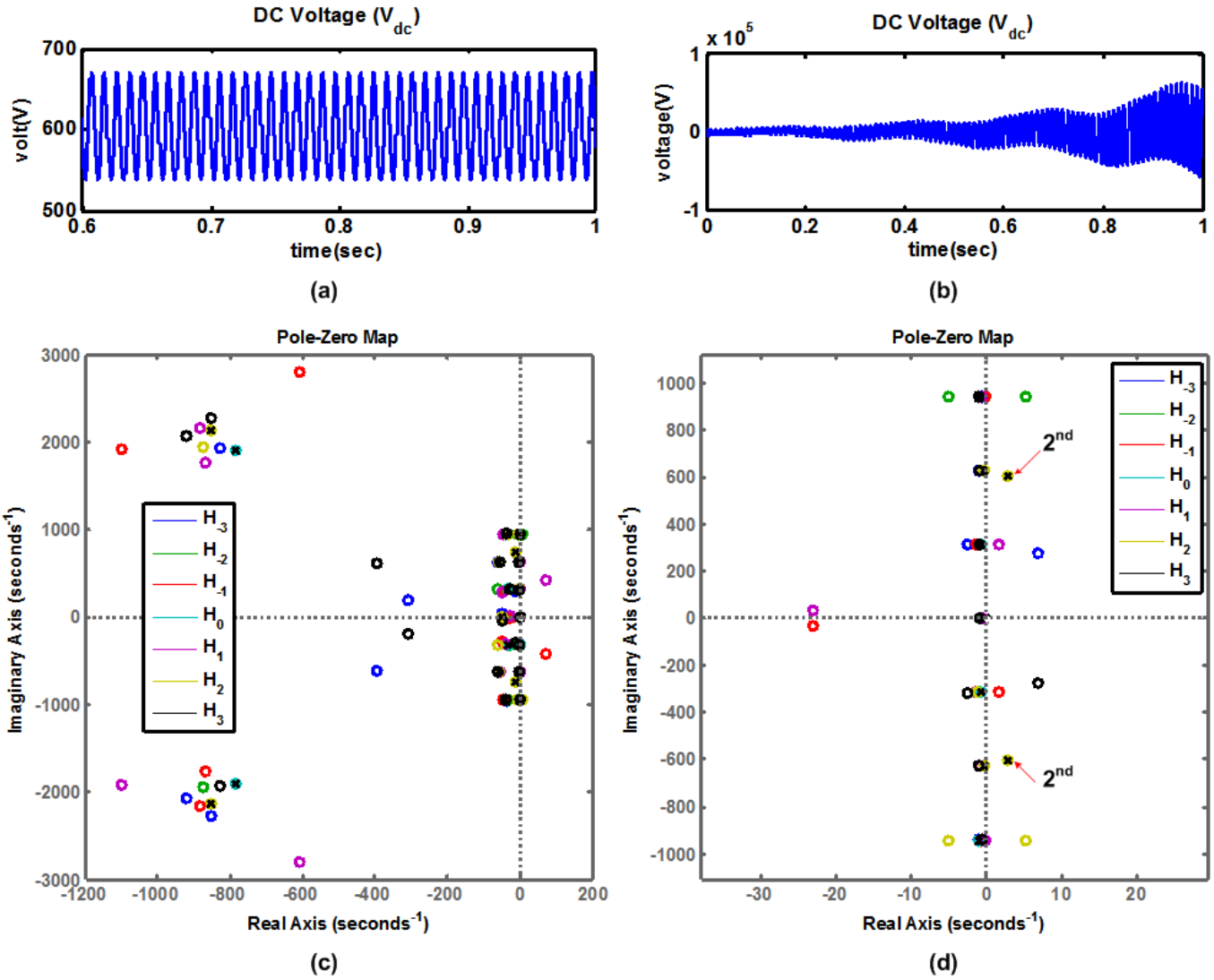


Fig 5. Dynamic simulation result of a single phase grid connected converter (10kW), where $H_k(s)$ is the harmonic transfer function (k= -3~3 ) (a) Time domain simulations of the HSS model (in stable case, $K_p$=0.5), (b) Time domain simulations of the HSS model (unstable case, $K_p$=3), (c) Pole Zero map of HSS model (stable case, $K_p$=0.5), (c) Pole Zero mapping of the HSS model (unstable case, $K_p$=3)

converted by using the Discrete Fourier Transform (DFT). The same number of harmonics, which was considered in the HSS modeling, is only used from the decomposed data by means of a sorting algorithm. Then the achieved time-varying Fourier coefficients are inserted into the Harmonic Transfer Function (HTF), which is calculated by (5)-(12). The output of the HTF is also time-varying Fourier coefficients, which reflect the dynamics of the single-phase converter. Finally, the time-varying Fourier coefficient can be converted into the time-domain signal by means of the rotation of the phasor ($e^{jh\omega t}$). The obtained time-domain signals are finally compared with the measured signals in the final stage.

The HSS results are shown in Fig. 8 which are obtained from the harmonic matrix. They matched well the PLECS simulation results as shown in Fig. 8-(a). This means that the steady state harmonics matrix is able to model the coupled harmonics. Furthermore, the simulations are compared with the experimental results as shown in Fig. 8-(b), where the main harmonics match well except for the even harmonics. This can be explained by the dead time (<1us - 2us) and the error of FFT analysis. If the resolution of the FFT is increased, the error will be reduced. However, the calculation time to achieve the HTF model can be increased. Hence, the selection of the number of harmonics and the resolution of the FFT depend on the analysis, which harmonics is the main concern.

## V. Conclusion

This paper proposes a new modeling method for single-phase grid connected converter. The obtained results show the steady-state harmonic coupling in the harmonic matrix, where the main characteristic harmonic and varying harmonic characteristic according to the disturbance from grid as well as other connected system can be explained by the HSS model. Besides, the derived harmonic transfer function can show

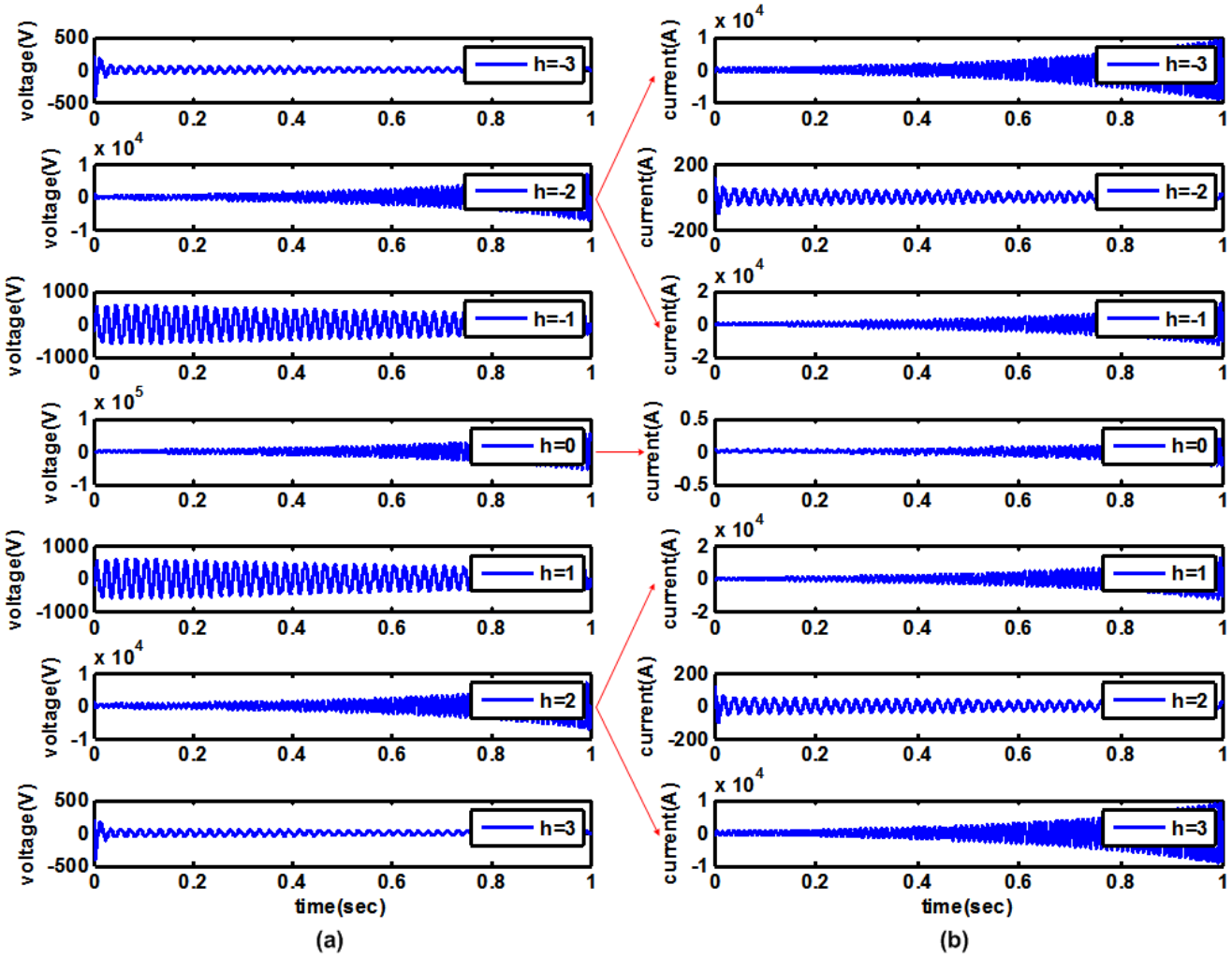


Fig 6. Dynamic harmonic response of single phase grid connected converter (10 kW), where h is the harmonic order (h=-3~3), (a) Harmonic response of dc side from HTF, (b) harmonic response of ac side from HTF

other dynamic performance with the traditional LTI based analysis method.

## ACKNOWLEDGMENT

This work was supported by European Research Council under the European Union's Seventh Framework Program (FP/2007-2013)/ERC Grant Agreement n. [321149-Harmony].

## REFERENCES

[1] S. B. Kjaer, J. K. Pedersen, and F. Blaabjerg, "A review of single-phase grid-connected inverters for photovoltaic modules," *IEEE Trans. on Ind. Appl.,* vol. 41, pp. 1292-1306, 2005.

[2] H. Jinwei, L. Yun Wei, D. Bosnjak, and B. Harris, "Investigation and resonances damping of multiple PV inverters," in *Proc. of IEEE APEC 2012*, 2012, pp. 246-253.

[3] D. G. Infield, P. Onions, A. D. Simmons, and G. A. Smith, "Power quality from multiple grid-connected single-phase inverters," *IEEE Trans. on Power Delivery,,* vol. 19, pp. 1983-1989, 2004.

[4] E. P. I. Association. Global market outlook for photovoltaics 2013-2017 [Online]. Available: http://www.epia.org/

[5] K.O.Kovanen, *Photovoltaics and power distribution*, May/Jun ed. vol. 14: Renewable Energy Focus, 2013.

[6] K. Ogimoto, I. Kaizuka, Y. Ueda, and T. Oozeki, "A Good Fit: Japan's Solar Power Program and Prospects for the New Power System," *IEEE, Power and Energy Magazine.,* vol. 11, pp. 65-74, 2013.

[7] C. Winneker. World`s solar photovoltaic capacity passes 100-gigawatt landmark after strong year [Online]. Available: http://www.epia.org/news/

[8] H. Jinwei, L. Yun Wei, D. Bosnjak, and B. Harris, "Investigation and Active Damping of Multiple Resonances in a Parallel-Inverter-Based Microgrid," *IEEE Trans. Power Electron.,* vol. 28, pp. 234-246, 2013.

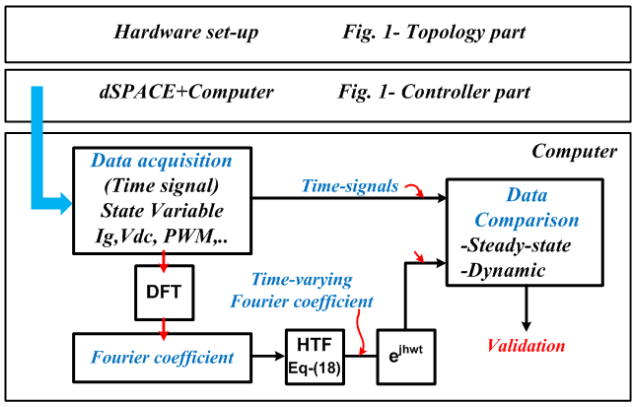


Fig 7. Block Diagram for the experimental validation of the HSS model (HTF)


[9] W. Xiongfei, F. Blaabjerg, and L. Poh Chiang, "Virtual RC Damping of LCL-Filtered Voltage Source Converters With Extended Selective Harmonic Compensation," *IEEE Trans. on Power Electron.,* vol. 30, pp. 4726-4737, 2015.

[10] W. Xiongfei, P. Ying, L. Poh Chiang, and F. Blaabjerg, "A Series LC-Filtered Active Damper With Grid Disturbance Rejection for AC Power-Electronics-Based Power Systems," *IEEE Trans. on Power Electron.,* vol. 30, pp. 4037-4041, 2015.

[11] R. Bojoi, L. R. Limongi, D. Roiu, and A. Tenconi, "Enhanced Power Quality Control Strategy for Single-Phase Inverters in Distributed Generation Systems," *IEEE Trans. Power Electron.,* vol. 26, pp. 798-806, 2011.

[12] A. Kulkarni and V. John, "Mitigation of Lower Order Harmonics in a Grid-Connected Single-Phase PV Inverter," *IEEE Trans. Power Electron.,* vol. 28, pp. 5024-5037, 2013.

[13] B. C. Smith, N. R. Watson, A. R. Wood, and J. Arrillaga, "A Newton solution for the harmonic phasor analysis of AC/DC converters," *IEEE Trans. on Power Delivery,,* vol. 11, pp. 965-971, 1996.

[14] S. R. Sanders, J. M. Noworolski, X. Z. Liu, and G. C. Verghese, "Generalized averaging method for power conversion circuits," *IEEE Trans. Power Electron.,* vol. 6, pp. 251-259, 1991.

[15] N. Kroutikova, C. A. Hernandez-Aramburo, and T. C. Green, "State-space model of grid-connected inverters under current control mode," *IET, Electric Power Applications,* vol. 1, pp. 329-338, 2007.

[16] M. S. P. Hwang and A. R. Wood, "A new modelling framework for power supply networks with converter based loads and generators - the Harmonic State-Space," in *Proc. of IEEE POWERCON*, 2012, pp. 1-6.

[17] G. N. Love and A. R. Wood, "Harmonic State Space model of power electronics," in *Proc. IEEE ICHQP*, 2008, pp. 1-6.


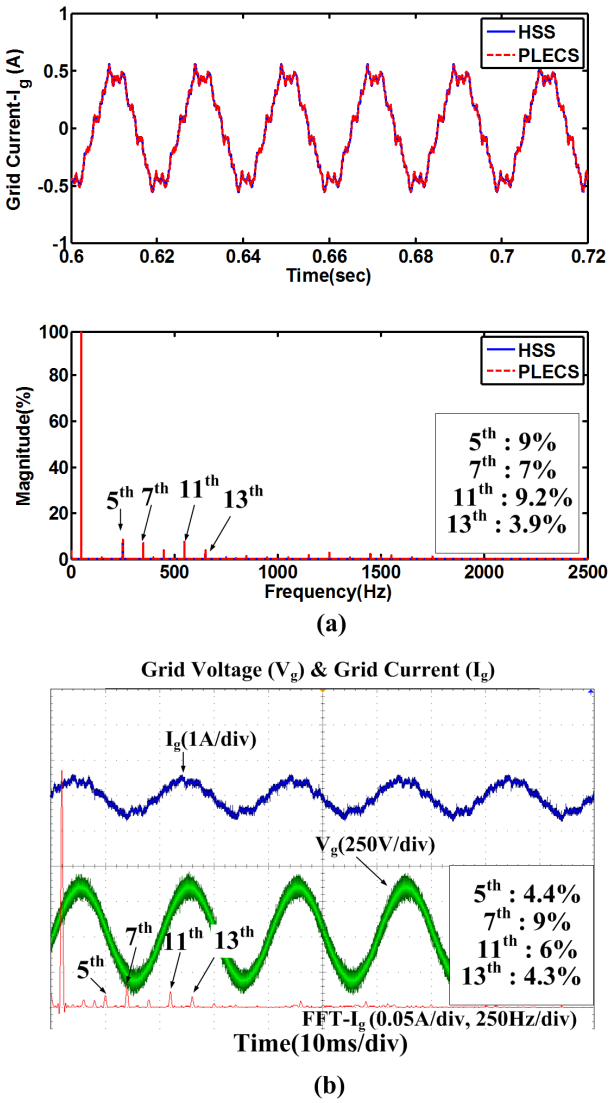


Fig 8. Simulation and experimental results for 1 kW power rating : Converter side inductor $L_f$ = 3 mH, grid side inductor $L_g$ = 1 mH, filter capacitance $C_f$ = 4.7 uF, dc link capacitor = 450 uF, dc link voltage = 450V, Grid Voltage = 230 V, switching frequency = 10 kHz) – Grid side inductor current simulation (harmonic = -40$^{th}$ – 40$^{th}$ ) waveform
(a) Simulation in HSS and PLECS (grid side inductor current (Ig) 0.5 A injection), (b) Experimental results of grid side inductor current (Ig) 0.5 A injection (blue = grid side current, green = grid voltage, red= FFT waveform of grid side current)


[18] N. M. Wereley and S. R. Hall, "Linear Time Periodic Systems: Transfer Function, Poles, Transmission Zeroes and Directional Properties," in *Proc. of IEEE ACC*, 1991, pp. 1179-1184.

[19] N. M. Wereley and S. R. Hall, "Frequency response of linear time periodic systems," in *Proc. of IEEE CDC*, 1990, pp. 3650-3655 vol.6.